Published in final edited form as:
Biochemistry. 2012 June 19; 51(24): 4968–4979. doi:10.1021/bi300498c.

Crystal Structures of *Trypanosoma cruzi* UDP-Galactopyranose Mutase Implicate Flexibility of the Histidine Loop in Enzyme Activation

Richa Dhatwalia[†,‖], **Harkewal Singh**[†,‖], **Michelle Oppenheimer**[#], **Pablo Sobrado**[#], and **John J. Tanner**[†,‡,*]

[†]Department of Chemistry, University of Missouri-Columbia, Columbia, MO 65211, USA

[#]Department of Biochemistry, Virginia Tech, Blacksburg, VA 24061, USA

[‡]Department of Biochemistry, University of Missouri-Columbia, Columbia, MO 65211, USA

Abstract

Chagas disease is a neglected tropical disease caused by the protozoan parasite *Trypanosoma cruzi*. Here we report crystal structures of the galactofuranose biosynthetic enzyme UDP-galactopyranose mutase (UGM) from *T. cruzi*, which are the first structures of this enzyme from a protozoan parasite. UGM is an attractive target for drug design because galactofuranose is absent in humans but is an essential component of key glycoproteins and glycolipids in trypanosomatids. Analysis of the enzyme-UDP noncovalent interactions and sequence alignments suggests that substrate recognition is exquisitely conserved among eukaryotic UGMs and distinct from that of bacterial UGMs. This observation has implications for inhibitor design. Activation of the enzyme via reduction of the FAD induces profound conformational changes, including a 2.3-Å movement of the histidine loop (Gly60-Gly61-His62), rotation and protonation of the imidazole of His62, and cooperative movement of residues located on the *si* face of the FAD. Interestingly, these changes are substantially different from those described for *Aspergillus fumigatus* UGM, which is 45 % identical to *T. cruzi* UGM. The importance of Gly61 and His62 for enzymatic activity was studied with the site-directed mutant enzymes G61A, G61P, and H62A. These mutations lower the catalytic efficiency by factors of 10–50, primarily by decreasing k_{cat}. Considered together, the structural, kinetic, and sequence data suggest that the middle Gly of the histidine loop imparts flexibility that is essential for activation of eukaryotic UGMs. Our results provide new information about UGM biochemistry and suggest a unified strategy for designing inhibitors of UGMs from the eukaryotic pathogens.

Chagas disease (aka American trypanosomiasis) is a major global health concern (1). The disease is caused by the protozoan parasite *Trypanosoma cruzi* and spread by triatomine insects, which carry the parasite in their gut. Chagas disease is one of several neglected tropical diseases, i.e., chronic infectious diseases that are prevalent in poor countries and

Corresponding author: Department of Chemistry, University of Missouri-Columbia, Columbia, MO 65211, USA; tannerjj@missouri.edu; phone: 573-884-1280; fax: 573-882-2754.

‖These authors contributed equally to this work.

ASSOCIATED CONTENT

Supporting Information

Figures showing steady-state kinetic profiles and the AfUGM tetramer are provided. This material is available free of charge via the Internet at http://pubs.acs.org.

Accession Codes

Atomic coordinates and structure factors been deposited in the Protein Data Bank under the following accession codes: 4DSG, oxidized TcUGM-UDP; 4DSH, reduced TcUGM-UDP.

underemphasized by society relative to the number of people affected. The disease is endemic in Latin America, and at least 10 million people worldwide are estimated to be infected with *T. cruzi* (1). Infection mainly occurs through contact with the feces of triatomine bugs, but transmission also occurs via blood transfusions, organ transplants, ingestion of contaminated food, and mother-to-child (1). It is estimated that 30 % of Chagas patients will develop heart damage in the late chronic stage of the disease, leading to death caused by arrhythmia in early adulthood (1). More than 10000 deaths occur annually from Chagas disease, and the burden of disease is the highest for any parasitic disease in the Western hemisphere (1, 2). Chagas is unusual among neglected diseases in that it is spreading to non-endemic areas, including the United States, Canada, and Europe (2, 3). The two drugs used for treatment, benznidazole and nifurtimox, have significant side effects and uncertain efficacy (4–6), and there is no vaccine available. The prevalence of the disease, the spread to new regions of the globe, and the lack of adequate medications emphasize the need for new drugs to treat Chagas disease.

The flavoenzyme UDP-galactopyranose mutase (UGM) has received attention recently as a drug design target for neglected tropical diseases (7–9). UGM plays a central role in the biosynthesis of galactofuranose (Gal*f*) by catalyzing the conversion of UDP-galactopyranose (UDP-Gal*p*) to UDP-galactofuranose (UDP-Gal*f*) (Figure 1). Galf has never been found in humans but is an essential component of the cell wall and extracellular matrix of many pathogenic bacteria, fungi, and protozoa (8, 9).

UGM and Gal*f* are widely distributed in pathogenic protozoa (7, 8). In particular, Gal*f* is present in glycoinositolphospholipids and glycosylphosphatidylinositol anchor proteins of *T. cruzi* (10, 11). In the related parasite, *Leishmania major*, which causes leishmaniasis, Gal*f* is present in the membrane anchor of the lipophosphoglycan and in glycoinositolphospholipids (12). These glycoconjugates are highly expressed throughout the life cycle of these parasites and are important for their survival and proliferation (12–14). Gal*f*-containing glycoconjugates are thought to be involved in the mechanism of myocardiac invasion by *T. cruzi* (15). In *Leishmania*, lipophosphoglycans are essential for the binding and detachment of the parasite to the midgut of the vector insect and thus for transmission of the parasite to the human host (16, 17). Furthermore, studies with lipophosphoglycan deletion mutants in *L. major* demonstrated that these glycosylated structures are involved in resistance to oxidative stress and evasion of the human immune system (16, 17). Moreover, a UGM deletion mutant of *L. major* exhibits attenuated virulence (7). In summary, Gal*f*-containing molecules of protozoan parasites function in host-specific cell recognition, growth, and pathogenesis. Since UGM is essential for the biosynthesis of Gal*f*, inhibition of the enzyme is an attractive approach for finding new drugs for Chagas disease and leishmaniasis.

The potential for inhibitor design and the uniqueness of the chemical mechanism of UGM have motivated structural studies of the enzyme. Several crystal structures of bacterial UGMs have been determined (18–23). These structures revealed the essential UGM fold and provided insight into several aspects of UGM biochemistry, including the structural basis of substrate recognition and the catalytic mechanism. Eukaryotic UGMs have received less attention. We recently reported crystal structures and small-angle X-ray scattering analysis of UGM from the pathogenic fungus *Aspergillus fumigatus* (AfUGM), which was the first structural data for any eukaryotic UGM (24). Shortly thereafter, Sanders' group published structures of AfUGM based on a different (space group *P*1) crystal form (25). Our analysis of the data showed that AfUGM has several extra secondary and tertiary structural elements that are not found in bacterial UGMs yet are important for substrate recognition and tetramerization (24). The AfUGM structures also revealed large conformational changes that accompany substrate binding, which is highly relevant for inhibitor design (24).

As part of our ongoing studies of UGM from eukaryotic pathogens, we report crystal structures of oxidized and reduced *T. cruzi* UGM (TcUGM) complexed with the inhibitor UDP. Analysis of the UDP binding site suggests a common strategy for designing inhibitors of UGMs from eukaryotic pathogens, including *T. cruzi*, *L. major*, and *A. fumigatus*. Comparison of the structures of oxidized and reduced TcUGM reveals profound conformational changes induced by reduction of the FAD cofactor, which provides new information about the molecular mechanism of enzyme activation by reducing agents. These results provide a foundation for inhibitor design and insight into UGM biochemistry.

EXPERIMENTAL PROCEDURES

Crystallization

TcUGM was expressed and purified as described previously (26). Crystallization studies used TcUGM at 7 – 8 mg/mL in 150 mM NaCl buffered at pH 7.5 with either 50 mM phosphate or 50 mM HEPES. Prior to crystallization, the enzyme was incubated with 10 mM UDP for 30 minutes. Crystallization experiments were performed at 20 °C using sitting drop vapor diffusion with the drops formed by mixing 1.5 μL each of the protein and reservoir solutions. Several commercially available crystallization screens were used to identify initial crystallization conditions. Promising conditions were obtained with reservoirs containing ammonium sulfate and HEPES buffer. Small yellow crystals appeared after 2 weeks. Larger crystals were obtained within a week via microseeding. The optimized crystallization reservoir contains 1.0 M ammonium sulfate, 0.5% polyethylene glycol 8000, and 0.1 M HEPES at pH 7.5. The crystals were cryoprotected in 1.2 M ammonium sulfate, 0.1 M HEPES pH 7.5, and 25% glycerol before plunging into liquid N_2.

The space group is $P6_522$ with unit cell dimensions of a = 143 Å and c = 354 Å. Based on the method of Matthews (27) and assuming ~ 50 % solvent content, the asymmetric unit is predicted to contain four protein molecules, which implies V_M of 2.4 $Å^3$/Da (48 % solvent). However, molecular replacement calculations show that the asymmetric unit contains just two protein molecules (*vide infra*), which corresponds to 74 % solvent and V_M of 4.8 $Å^3$/Da.

Crystals of the TcUGM-UDP complex with the FAD in the reduced state were prepared by soaking the aforementioned crystals in 1.2 M ammonium sulfate, 0.1 M HEPES pH 7.5, 60 mM sodium dithionite, and 25% ethylene glycol. Once the crystals turned from yellow to colorless, they were flash-cooled by plunging into liquid N_2.

X-ray Diffraction Data Collection, Phasing, and Refinement

Diffraction data were collected at the Advanced Photon Source. The data set for oxidized TcUGM-UDP was collected at beamline 19-ID and processed using HKL3000 (28). The data set for reduced TcUGM-UDP was collected at beamline 24-ID-C, and the data were integrated using XDS (29) and scaled with SCALA (30) via CCP4i (31). Data processing statistics are listed in Table 1.

The phase problem for oxidized TcUGM-UDP was solved using molecular replacement as implemented in MOLREP (32). The search model was derived from the structure of AfUGM (PDB code 3UTE(24)). Chainsaw was used to create a model in which all the side chains were pruned to the β carbon atom. The calculations produced a solution having two molecules in the asymmetric unit with R-factor of 0.6 and score of 0.3. The model was manually edited and built using COOT (33) and refined using PHENIX (34). An advanced model of oxidized TcUGM-UDP was used as the starting point for refinement of reduced TcUGM-UDP. Refinement statistics are listed in Table 1. We note that, for both the

oxidized and reduced TcUGM-UDP structures, the two molecules in the crystallographic asymmetric unit are identical within experimental error.

Mutagenesis and Kinetics

The site directed mutant enzymes G61A, G61P, and H62A were created using the QuikChange Site-Directed Mutagenesis Kit (Stratagene) following the protocol supplied by the manufacturer. All the mutants were expressed and purified following the procedures previously described for the wild-type enzyme (26).

The activities of the TcUGM mutant enzymes G61A, G61P, and H62A were determined using steady-state kinetics analysis as described previously (26, 35). In these experiments, the rate of conversion of UDP-Gal*f* to UDP-Gal*p* was measured at 37°C and pH 7.5 in the presence of 20 mM dithionite. The reverse reaction was studied because the equilibrium between UDP-Gal*p* and UDP-Gal*f* favors the former by the ratio of 13:1. Synthesis of UDP-Gal*f* was performed as described previously (26, 36).

RESULTS

Overall Fold and Oligomeric State

The structures of oxidized and reduced TcUGM complexed with the inhibitor UDP were determined at 2.25 Å resolution (Table 1). These are the first structures of UGM from a parasitic pathogen and the second structure of a eukaryotic UGM.

TcUGM has a mixed α/β fold that comprises three domains (Figure 2A). Domain 1 is the largest and consists of three sections of the polypeptide chain (residues 4–86, 199–291, 397–475). This domain functions primarily in binding FAD and has a Rossmann fold as its core. Domain 2 is a bundle of α-helices and participates in substrate binding (residues 101–198). Domain 3 features a twisted, 7-stranded β-sheet that sits atop a 15-residue α-helix (residues 87–100, 292–396). This domain also contributes to substrate binding.

AfUGM is the closest structural neighbor of TcUGM in the Protein Data Bank (PDB). The two enzymes are 45 % identical in sequence, and the two structures superimpose with a root mean square deviation of 1.1 Å (Figure 2B). Although they share a common overall fold, several local variations between the two structures are evident (Figure 2B). For example, a loop of domain 1 is longer in TcUGM, whereas a loop in domain 3 is longer in AfUGM. The significance of these differences is not obvious. In contrast, other differences are substantive in that they appear to dictate the oligomeric state formed in solution (see Discussion). These include the longer α-helix in domain 2 of AfUGM and the additional α-helix at the C-terminus of AfUGM (Figure 2B).

The crystal structure is consistent with TcUGM being monomeric in solution. Analysis of protein-protein interfaces in the crystal lattice using the PDBePISA (37) revealed no oligomers predicted to be stable in solution. Furthermore, neither the AfUGM tetramer nor its constituent dimers are present in the TcUGM crystal lattice. Moreover, none of the dimeric assemblies of bacterial UGMs are observed in the lattice. It is concluded that TcUGM forms a monomer in solution, which is consistent with recent size exclusion chromatography data (26).

Binding of UDP

The structures of TcUGM complexed with UDP were determined from crystals that had been grown in the presence of the inhibitor. Electron density maps clearly indicated that UDP is bound in the active site with full occupancy (Figure 3A). The protein-ligand

interactions are identical in the reduced and oxidized enzymes, so we will focus on the reduced enzyme complex.

UDP binds at the *re* face of the isoalloxazine and is covered by the 170s and 200s flaps (Figure 2A). Structures of AfUGM showed that the analogous loops move by 10 Å from the open to closed conformation upon UDP binding. The flaps of TcUGM-UDP are in the closed conformation, as expected. Although it was not possible to crystallize TcUGM in the ligand-free state, presumably the 170s and 200s flaps open and close as in AfUGM.

UDP forms several interactions with TcUGM (Figure 3). The uracil ring is wedged between the aromatic rings of Tyr100 and Phe152, which positions the base to form three hydrogen bonds with the side chain of Gln103 and backbone of Phe102. Thus the hydrogen bonding potential of uracil is fully satisfied. The ribose hydroxyl groups of UDP interact with Asn157 and Trp161. The pyrophosphate directly interacts with Arg327 and three tyrosine residues (317, 395, and 429). Several water-mediated hydrogen bonds are also observed. In summary all three chemical groups of UDP - base, ribose, and pyrophosphate - are in direct electrostatic contact with the enzyme, which results in a plethora of stabilizing interactions.

Conformational Changes Induced by FAD Reduction

The FAD of UGM functions as a nucleophile that attacks the anomeric carbon atom of the galactose moiety (C1 in Figure 1) in an S_N2-like reaction, thus enzymatic activity requires that the FAD be in the reduced state ($FADH^-$) (26, 38, 39). Structures of oxidized and reduced TcUGM were determined to understand the mechanism by which the enzyme is activated by FAD reduction.

The structure of the oxidized enzyme was determined from crystals that were grown and cryoprotected without reducing agent. These crystals were yellow, which is characteristic of the oxidized state of FAD. The structure of the reduced enzyme was determined from crystals of the oxidized enzyme that were soaked in reducing agent (dithionite) prior to flash-cooling in liquid nitrogen. The crystals turned colorless during soaking, which indicated that the FAD was reduced.

Reduction of the FAD causes substantial conformational changes in the active site (Figure 4). In the oxidized enzyme, the conserved histidine loop (Gly60-Gly61-His62) adopts an unprecedented conformation for UGMs in which it is retracted from the FAD isoalloxazine (Figure 4A). This conformation is stabilized by hydrogen bonds between Asp58 and the backbone of Gly61 and His62. Upon reduction, the histidine loop shifts 2.3 Å toward the isoalloxazine (Figure 4B). In this conformation, the carbonyl of Gly61 accepts a hydrogen bond from the flavin N5, which is a hydrogen bond donor in the reduced state. This hydrogen bond is observed in all reduced UGM structures and is thus thought to be essential for stabilizing the reduced flavin. Movement of the histidine loop toward the reduced flavin triggers other conformational changes (Figure 4C). Asp58 and Thr212 rotate to engage each other in a hydrogen bond. Note that the rotation of Asp58 also allows a hydrogen bond with Ser 48. Finally, Met347 moves into the space vacated by Gly61 and Asp58, while Gln434 rotates away from His62.

The imidazole ring of His62 becomes protonated and flips by 180° upon flavin reduction. Although the protonation state and value of $\chi 2$ of histidine cannot be determined solely from electron density at 2.25 Å resolution, these attributes can be inferred from hydrogen bonding considerations and knowledge of the preferred tautomer of neutral histidine. Analysis of hydrogen bonding with MolProbity (40) suggests that in the oxidized enzyme, His62 adopts the neutral τtautomer with the imidazole accepting a hydrogen bond from Gln434 and donating a hydrogen bond to the carbonyl of Leu59 (Figure 4A). We note that τ

is the preferred tautomer of neutral His (41). In the reduced enzyme, on the other hand, hydrogen bonding is maximized with the imidazole protonated and flipped by 180° to allow hydrogen bonds with the carbonyl of Gly60 and the FAD 2'-hydroxyl (Figure 4B). Note that the assigned protonation states of His62 are consistent with the fact that the oxidized FAD is uncharged and the reduced FAD is anionic ($FADH^-$).

Reduction also affects the conformation of the isoalloxazine (Figure 5). In the oxidized state, the electron density maps are consistent with a planar isoalloxazine (Figure 5A). In the reduced enzyme, the FAD exhibits a butterfly-like conformation in which the pyrimidine ring bends 7° out of the plane such that the *si* face is concave (Figure 5B). This conformation is identical to that of reduced AfUGM.

Site-directed Mutagenesis of the Histidine Loop

The importance of the histidine loop for catalytic activity was investigated using site-directed mutagenesis. Gly61 and His62 were targeted for mutagenesis because they form hydrogen bonds to $FADH^-$ and exhibit large conformational changes upon flavin reduction. Gly61 is conserved among eukaryotic UGMs but appears as Ala or Pro in bacterial UGMs. Therefore, the mutant enzymes G61A and G61P were created. His62 is universally conserved among UGMs, and the H62A mutant enzyme was created. (For reference, Gly60 is also conserved in all UGMs.)

Mutation of the histidine loop of TcUGM is highly detrimental to activity (Figure S1 of Supporting Information and Table 2). Mutation of Gly61 to Ala reduces k_{cat} by a factor of 70 but reduces K_m by only a factor of 3. As a result, the catalytic efficiency of G61A is only 4% of that of TcUGM. Similarly, mutation of Gly61 to Pro substantially decreases k_{cat} (factor of 16) but has less effect on K_m. The catalytic efficiency of this mutant enzyme is 10% of that of TcUGM. Mutation of His62 to Ala has a profound effect on k_{cat}; this mutation decreases k_{cat} by over 300. The catalytic efficiency of H62A is just 2 % compared to that of TcUGM. These results suggest that Gly and His at positions 61 and 62 are important for efficient catalysis by TcUGM. Furthermore, the histidine loop sequences found in bacterial UGMs (GAH, GPH) are poorly tolerated by TcUGM.

DISCUSSION

Inhibitor design is aided by knowledge of substrate recognition, and substrate recognition appears to be exquisitely conserved among eukaryotic UGMs. Comparison of the structures of TcUGM and AfUGM complexed with UDP show that the UDP binding sites are identical (Figure 6). All residues that contact UDP, either directly or via water molecules, are present in both enzymes. Furthermore, the conformations of these residues, as well as their interactions with UDP, are identical in the two structures. The structural similarity extends even to the water molecules that mediate protein-inhibitor interactions (Figure 6). Moreover, all residues that contact UDP or UDP-Gal*p* in the TcUGM and AfUGM crystal structures are also present in many other eukaryotic UGMs, including *L. major* UGM (Figure 7, triangles). Thus, it is likely that the AfUGM and TcUGM structures are representative of eukaryotic UGMs with regard to substrate binding.

This analysis suggests a unified strategy for designing inhibitors of UGMs from *T. cruzi*, *L. major*, and *A. fumigatus*, which are three important eukaryotic pathogens. For example, a compound that binds in the active site of any of these enzymes is predicted to also inhibit the other ones. Therefore, screening efforts could be focused on one enzyme. Our results also suggest that testing known inhibitors of bacterial UGMs may not be an optimal strategy for identifying inhibitors of eukaryotic UGMs. We previously showed that the substrate site of eukaryotic UGMs differs substantially from that of bacterial UGMs, particularly in the

region around the UMP moiety (see Figure S2 of Dhatwalia *et al.* (24)). Thus, compounds that target the UMP site of bacterial UGMs will not likely have high affinity for eukaryotic UGMs. In summary, the very high structural similarity of the substrate binding sites of TcUGM and AfUGM raises the possibility of finding a single compound that inhibits multiple eukaryotic UGMs. This observation simplifies inhibitor discovery.

The structures also provide insight into the surprising lack of conservation of the oligomeric state by eukaryotic UGMs. TcUGM is the first example of a monomeric UGM. As we reported previously (24), AfUGM forms a dimer-of-dimers tetramer having 222 point group symmetry (Figure S2 of Supporting Information). Three conformational differences between the two enzymes account for the difference in oligomeric state. First, AfUGM has an additional 7-residue α-helix at the C-terminus (Figure 2B), and this helix packs against domain 1 of another protomer in the tetramer (Figure S2 of Supporting Information). The absence of this helix in TcUGM obviously precludes formation of this critical interface. The second point of departure occurs in the two parallel helices of domain 2 (Figure 2C). These helices form an intersubunit 4-helix bundle across one of the two-fold axes in the AfUGM tetramer (Figure S2B of Supporting Information). The 4-helix bundle in AfUGM has a tightly packed hydrophobic interior. In contrast, TcUGM has long charged and polar side chains on these helices, which would inhibit formation of the hydrophobic bundle (Figure 2C). In particular, if a theoretical tetramer is built from TcUGM monomers, Arg186, Arg114, and Gln190 form steric clashes with the symmetry related helices. The potential for these clashes presumably prevents TcUGM from forming this interface. Finally, TcUGM is unable to form the four intersubunit hydrogen bonds that are present in the centroid of the AfUGM tetramer (Figure S2A of Supporting Information, inset). These hydrogen bonds involve Arg133, which is located at the C-terminus of one of the helices of the 4-helix bundle (Figure 2C). Because the helix is a full turn shorter in TcUGM, these intersubunit interactions cannot be formed. These conformational differences account for the difference in the oligomeric states of TcUGM and AfUGM.

The TcUGM structures provide new information about conformational changes associated with activation of the enzyme via reduction of the FAD (Figures 4 and 5). Reduction of the FAD causes several concerted changes in the protein. The histidine loop moves by 2.3 Å (Figure 4C). His62, a universally conserved residue in UGMs, flips by 180° and becomes protonated. The protonation of His62 may help stabilize the negative charge of the reduced FAD. The side chains of Asp58 and Thr212 rotate by 180°. Met 347 and Gln434 move by 1.6 Å. It is notable that all of these residues are located on the side of the FAD that is opposite to the substrate-binding site. Thus, two critical aspects of function are delegated to distinct regions of the protein: maintaining the redox state is the responsibility of residues on the *si* face FAD, while substrate binding is performed by residues on the *re* side.

These conformational changes are consistent with the generally accepted chemical mechanism of UGM. The prevailing mechanism is an S_N2-type displacement in which the N5 atom of the reduced FAD functions as the nucleophile that attacks the anomeric carbon of galactose to form a covalent intermediate and displace UDP (38, 39). This mechanism was recently validated for TcUGM (26). Activity thus requires that the FAD be reduced. The coordinated movements of the histidine loop, Asp58, Thr212, and the FAD isoalloxazine in TcUGM have two salient effects. First, a hydrogen bond is created between the N5 atom of the reduced flavin and the carbonyl oxygen atom of the residue preceding the conserved histidine (Gly61). This interaction is seen in all reduced UGMs and is therefore thought to be essential for stabilizing the reduced flavin. Second, curvature is induced in the flavin isoalloxazine such that the *si* face is concave. Bending of the isoalloxazine in this direction is consistent with the FAD functioning as a nucleophile (19).

Curiously, the conformational changes observed for TcUGM are different from those described for the close homolog AfUGM (Figure 8). We previously reported structures of oxidized and reduced AfUGM based on a $P6_522$ crystal form (24). Sanders' group subsequently reported $P1$ structures of AfUGM (25). The structures of the reduced active sites are nearly identical in TcUGM and AfUGM (Figure 8C). However, in oxidized AfUGM, the His residue of the histidine loop is substantially displaced toward the pyrimidine portion of the isoalloxazine (Figure 8B), whereas in oxidized TcUGM the His residue is near the middle ring of the isoalloxazine (Figure 8A). Furthermore, in oxidized AfUGM, the carbonyl bond vector of the middle Gly residue is directed away from the isoalloxazine (Figure 8B, Gly62), whereas the corresponding carbonyl of oxidized TcUGM points toward the isoalloxazine (Figure 8A, Gly61). Reduction of the FAD in AfUGM causes a 6–8 Å movement of the imidazole ring of the conserved histidine (Figure 8). As described above, the movement of the histidine loop in TcUGM is more subtle. It should be noted that elucidation of redox-linked conformational changes for AfUGM is complicated by the adventitious binding of sulfate ions to the oxidized active site of the $P6_522$ crystal form (PDB code 3UTE) and weak electron density for the histidine loop and bound UDP in the oxidized $P1$ form (3UKH). Nevertheless, taken together, the AfUGM and TcUGM structures implicate flexibility of the histidine loop in the mechanism of enzyme activation.

The large conformational changes in the histidine loop observed in TcUGM and AfUGM appear to be unique to eukaryotic UGMs. Comparison of oxidized and reduced bacterial UGM structures shows that flavin reduction induces bending of the isoalloxazine but no substantial changes in the protein conformation (19, 21, 22). Analysis of amino acid sequence conservation provides a rationale for why the histidine loop is static in bacterial UGMs and dynamic in eukaryotic UGMs. The histidine loop sequence of GGH is conserved among eukaryotic UGMs (Figure 7). In contrast, bacterial UGMs have either Ala or Pro in place of the second Gly. The extra Gly in the histidine loop most likely accounts for the increased flexibility of the loop in AfUGM and TcUGM.

This additional flexibility of the histidine loop appears to be important for function in TcUGM. Our mutagenesis data show that transplanting the bacterial sequences of GAH and GPH into TcUGM substantially decreases catalytic efficiency (Table 2). It is possible that the additional flexibility afforded by the extra Gly residue in TcUGM is needed to establish optimal hydrogen bonding between the histidine loop and $FADH^-$. Although structures of the TcUGM histidine loop mutant enzymes are not available, it is possible that the loop-flavin hydrogen bonding is suboptimal in these impaired enzymes, which likely decreases the nucleophilic character of the reduced flavin. This idea is consistent with the markedly decreased k_{cat} values of the histidine loop mutants.

Why eukaryotic UGMs undergo such large conformational changes upon activation is an open question. One possibility is that these conformational changes control the access of O_2 and reductant to the flavin. In the reduced enzyme, positioning the histidine loop close to the isoalloxazine N5-C4a edge helps protect the C4a atom of the reduced FAD from attack by O_2 (Figure 4B). Retraction of the loop upon oxidation perhaps allows open space for reducing agents to gain access to the oxidized flavin (Figure 4A). Regulation of function is another possibility. Conformational changes that are linked to the flavin redox state often serve a regulatory purpose (42). Whether eukaryotic UGMs are subject to some sort of redox-linked regulation remains to be determined.

Supplementary Material

Refer to Web version on PubMed Central for supplementary material.

Acknowledgments

We thank Dr. Jonathan Schuermann and Dr. Norma Duke for help with X-ray diffraction data collection and processing. This work is based upon research conducted at the Advanced Photon Source on the Northeastern Collaborative Access Team beamlines, which are supported by award RR-15301 from the National Center for Research Resources at the National Institutes of Health. Use of the Advanced Photon Source was supported by the U. S. Department of Energy, Office of Science, Office of Basic Energy Sciences, under Contract No. DE-AC02-06CH11357.

This research was supported by NIH grant R01 GM094469 (to P.S. and J.J.T). M.O. was supported by American Heart Association predoctoral fellowship 10PRE4160020.

ABBREVIATIONS

UGM	UDP-galactopyranose mutase
UDP-Gal*p*	UDP-galactopyranose
UDP-Gal*f*	UDP-galactofuranose
TcUGM	UDP-galactopyranose mutase from *Trypanosoma cruzi*
AfUGM	UDP-galactopyranose mutase from *Aspergillus fumigatu*
PDB	Protein Data Bank

REFERENCES

1. Savioli, L.; Daumerie, D. First WHO report on neglected tropical diseases: working to overcome the global impact of neglected tropical diseases. In: Crompton, DWT., editor. Geneva: World Health Organization; 2010.
2. Bern C, Montgomery SP. An estimate of the burden of Chagas disease in the United States. Clin. infect. Dis. 2009; 49:e52–e54. [PubMed: 19640226]
3. Tanowitz HB, Weiss LM, Montgomery SP. Chagas disease has now gone global. PLoS Negl. Trop. Dis. 2011; 5:e1136. [PubMed: 21572510]
4. Bern C, Montgomery SP, Herwaldt BL, Rassi A Jr, Marin-Neto JA, Dantas RO, Maguire JH, Acquatella H, Morillo C, Kirchhoff LV, Gilman RH, Reyes PA, Salvatella R, Moore AC. Evaluation and treatment of chagas disease in the United States: a systematic review. JAMA. 2007; 298:2171–2181. [PubMed: 18000201]
5. Teixeira AR, Cordoba JC, Souto Maior I, Solorzano E. Chagas' disease: lymphoma growth in rabbits treated with Benznidazole. Am. J. Trop. Med. Hyg. 1990; 43:146–158. [PubMed: 2117856]
6. Issa VS, Bocchi EA. Antitrypanosomal agents: treatment or threat? Lancet. 2010; 376:768. author reply 768–769. [PubMed: 20816538]
7. Beverley SM, Owens KL, Showalter M, Griffith CL, Doering TL, Jones VC, McNeil MR. Eukaryotic UDP-galactopyranose mutase (GLF gene) in microbial and metazoal pathogens. Eukaryot. Cell. 2005; 4:1147–1154. [PubMed: 15947206]
8. Tefsen B, Ram AF, van Die I, Routier FH. Galactofuranose in eukaryotes: aspects of biosynthesis and functional impact. Glycobiology. 2011 in press.
9. Oppenheimer M, Valenciano AL, Sobrado P. Biosynthesis of galactofuranose in kinetoplastids: novel therapeutic targets for treating leishmaniasis and chagas' disease. Enzyme Res. 2011; 2011:1–13.
10. Almeida IC, Ferguson MA, Schenkman S, Travassos LR. GPI-anchored glycoconjugates from *Trypanosoma cruzi* trypomastigotes are recognized by lytic anti-alpha-galactosyl antibodies isolated from patients with chronic Chagas' disease. Braz. J. Med. Biol. Res. 1994; 27:443–447. [PubMed: 8081263]
11. Ralton JE, Milne KG, Guther ML, Field RA, Ferguson MA. The mechanism of inhibition of glycosylphosphatidylinositol anchor biosynthesis in *Trypanosoma brucei* by mannosamine. J. Biol. Chem. 1993; 268:24183–24189. [PubMed: 8226965]

12. Ferguson MA. The surface glycoconjugates of trypanosomatid parasites. Philos. Trans. R. Soc. Lond. B Biol. Sci. 1997; 352:1295–1302. [PubMed: 9355120]
13. Turnock DC, Ferguson MA. Sugar nucleotide pools of *Trypanosoma brucei*, *Trypanosoma cruzi*, and L*eishmania major*. Eukaryotic cell. 2007; 6:1450–1463. [PubMed: 17557881]
14. MacRae JI, Obado SO, Turnock DC, Roper JR, Kierans M, Kelly JM, Ferguson MA. The suppression of galactose metabolism in *Trypanosoma cruzi* epimastigotes causes changes in cell surface molecular architecture and cell morphology. Mol. Biochem. Parasitol. 2006; 147:126–136. [PubMed: 16569451]
15. Turner CW, Lima MF, Villalta F. *Trypanosoma cruzi* uses a 45-kDa mucin for adhesion to mammalian cells. Biochem. Biophys. Res. Commun. 2002; 290:29–34. [PubMed: 11779128]
16. Spath GF, Garraway LA, Turco SJ, Beverley SM. The role(s) of lipophosphoglycan (LPG) in the establishment of *Leishmania major* infections in mammalian hosts. Proc Natl Acad Sci U S A. 2003; 100:9536–9541. [PubMed: 12869694]
17. Zhang K, Barron T, Turco SJ, Beverley SM. The LPG1 gene family of *Leishmania major*. Mol. Biochem. Parasitol. 2004; 136:11–23. [PubMed: 15138063]
18. Sanders DA, Staines AG, McMahon SA, McNeil MR, Whitfield C, Naismith JH. UDP-galactopyranose mutase has a novel structure and mechanism. Nat. Struct. Biol. 2001; 8:858–863. [PubMed: 11573090]
19. Beis K, Srikannathasan V, Liu H, Fullerton SW, Bamford VA, Sanders DA, Whitfield C, McNeil MR, Naismith JH. Crystal structures of *Mycobacteria tuberculosis* and *Klebsiella pneumoniae* UDP-galactopyranose mutase in the oxidised state and *Klebsiella pneumoniae* UDP-galactopyranose mutase in the (active) reduced state. J. Mol. Biol. 2005; 348:971–982. [PubMed: 15843027]
20. Gruber TD, Borrok MJ, Westler WM, Forest KT, Kiessling LL. Ligand binding and substrate discrimination by UDP-galactopyranose mutase. J Mol Biol. 2009; 391:327–340. [PubMed: 19500588]
21. Gruber TD, Westler WM, Kiessling LL, Forest KT. X-ray crystallography reveals a reduced substrate complex of UDP-galactopyranose mutase poised for covalent catalysis by flavin. Biochemistry. 2009; 48:9171–9173. [PubMed: 19719175]
22. Partha SK, van Straaten KE, Sanders DA. Structural basis of substrate binding to UDP-galactopyranose mutase: crystal structures in the reduced and oxidized state complexed with UDP-galactopyranose and UDP. J. Mol. Biol. 2009; 394:864–877. [PubMed: 19836401]
23. Partha SK, Sadeghi-Khomami A, Slowski K, Kotake T, Thomas NR, Jakeman DL, Sanders DA. Chemoenzymatic synthesis, inhibition studies, and X-ray crystallographic analysis of the phosphono analog of UDP-Galp as an inhibitor and mechanistic probe for UDP-galactopyranose mutase. J. Mol. Biol. 2010; 403:578–590. [PubMed: 20850454]
24. Dhatwalia R, Singh H, Oppenheimer M, Karr DB, Nix JC, Sobrado P, Tanner JJ. Crystal structures and small-angle X-ray scattering analysis of UDP-galactopyranose mutase from the pathogenic fungus *Aspergillus fumigatus*. J. Biol. Chem. 2012; 287:9041–9051. [PubMed: 22294687]
25. van Straaten KE, Routier FH, Sanders DA. Structural insight into the unique substrate binding mechanism and flavin redox state of UDP-galactopyranose mutase from *Aspergillus fumigatus*. J. Biol. Chem. 2012; 287:10780–10790. [PubMed: 22334662]
26. Oppenheimer M, Valenciano AL, Kizjakina K, Qi J, Sobrado P. Chemical Mechanism of UDP-Galactopyranose Mutase from *Trypanosoma cruzi*: A Potential Drug Target against Chagas' Disease. PLoS ONE. 2012; 7:e32918. [PubMed: 22448231]
27. Matthews BW. Solvent content of protein crystals. J. Mol. Biol. 1968; 33:491–497. [PubMed: 5700707]
28. Otwinowski Z, Minor W. Processing of X-ray diffraction data collected in oscillation mode. Methods Enzymol. 1997; 276:307–326.
29. Kabsch W. XDS. Acta Crystallogr. D Biol. Crystallogr. 2010; 66:125–132. [PubMed: 20124692]
30. Evans P. Scaling and assessment of data quality. Acta Crystallogr. D Biol. Crystallogr. 2006; 62:72–82. [PubMed: 16369096]
31. Potterton E, Briggs P, Turkenburg M, Dodson E. A graphical user interface to the CCP4 program suite. Acta Crystallogr D Biol Crystallogr. 2003; 59:1131–1137. [PubMed: 12832755]

32. Vagin A, Teplyakov A. MOLREP: an automated program for molecular replacement. J. Appl. Cryst. 1997; 30:1022–1025.
33. Emsley P, Cowtan K. Coot: model-building tools for molecular graphics. Acta Crystallogr. D Biol. Crystallogr. 2004; 60:2126–2132. [PubMed: 15572765]
34. Adams PD, Afonine PV, Bunkoczi G, Chen VB, Davis IW, Echols N, Headd JJ, Hung LW, Kapral GJ, Grosse-Kunstleve RW, McCoy AJ, Moriarty NW, Oeffner R, Read RJ, Richardson DC, Richardson JS, Terwilliger TC, Zwart PH. PHENIX: a comprehensive Python-based system for macromolecular structure solution. Acta Crystallogr. D Biol. Crystallogr. 2010; 66:213–221. [PubMed: 20124702]
35. Oppenheimer M, Poulin MB, Lowary TL, Helm RF, Sobrado P. Characterization of recombinant UDP-galactopyranose mutase from *Aspergillus fumigatus*. Arch. Biochem. Biophys. 2010; 502:31–38. [PubMed: 20615386]
36. Poulin MB, Lowary TL. Methods to study the biosynthesis of bacterial furanosides. Methods Enzymol. 2010; 478:389–411. [PubMed: 20816491]
37. Krissinel E, Henrick K. Inference of macromolecular assemblies from crystalline state. J. Mol. Biol. 2007; 372:774–797. [PubMed: 17681537]
38. Soltero-Higgin M, Carlson EE, Gruber TD, Kiessling LL. A unique catalytic mechanism for UDP-galactopyranose mutase. Nat Struct. Mol. Biol. 2004; 11:539–543. [PubMed: 15133501]
39. Sun HG, Ruszczycky MW, Chang WC, Thibodeaux CJ, Liu HW. Nucleophilic participation of the reduced flavin coenzyme in the mechanism of UDP-Galactopyranose mutase. J. Biol. Chem. 2011
40. Chen VB, Arendall WB 3rd, Headd JJ, Keedy DA, Immormino RM, Kapral GJ, Murray LW, Richardson JS, Richardson DC. MolProbity: all-atom structure validation for macromolecular crystallography. Acta crystallogr. Section D, Biological crystallography. 2010; 66:12–21.
41. Li S, Hong M. Protonation, tautomerization, and rotameric structure of histidine: a comprehensive study by magic-angle-spinning solid-state NMR. J Am Chem Soc. 2011; 133:1534–1544. [PubMed: 21207964]
42. Becker DF, Zhu W, Moxley MA. Flavin redox switching of protein functions. Antioxid Redox Signal. 2011; 14:1079–1091. [PubMed: 21028987]
43. Weiss M. Global indicators of X-ray data quality. J. Appl. Cryst. 2001; 34:130–135.
44. Engh RA, Huber R. Accurate bond and angle parameters for x-ray protein structure refinement. Acta Cryst. 1991; A47:392–400.
45. Lovell SC, Davis IW, Arendall WB 3rd, de Bakker PI, Word JM, Prisant MG, Richardson JS, Richardson DC. Structure validation by Calpha geometry: phi,psi and Cbeta deviation. Proteins. 2003; 50:437–450. [PubMed: 12557186]
46. DeLano, WL. The PyMOL User's Manual. Palo Alto, CA, USA: DeLano Scientific; 2002.

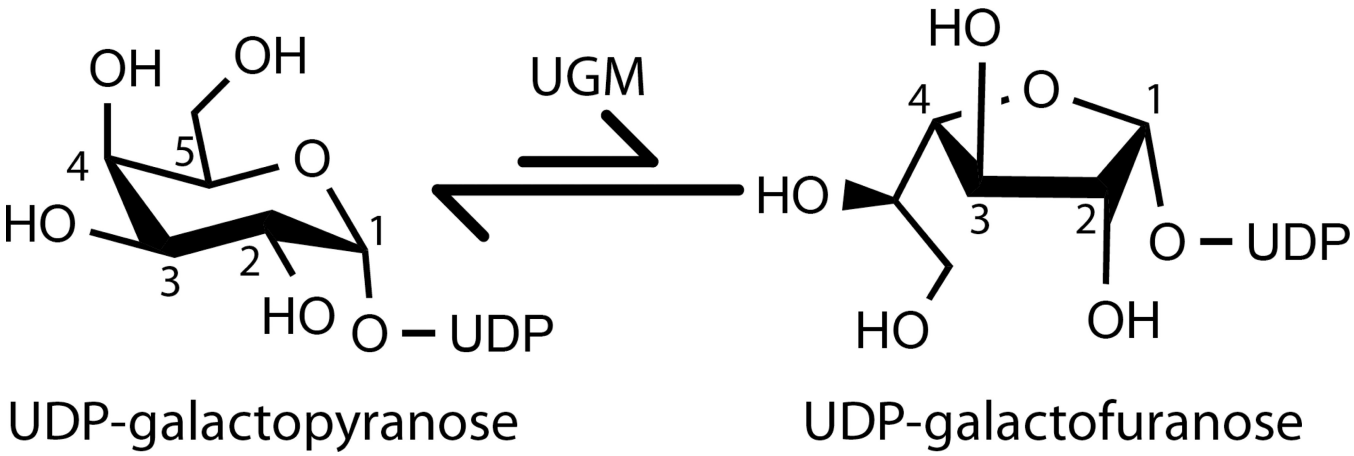

UDP-galactopyranose UDP-galactofuranose

Figure 1.
Reaction catalyzed by UGM.

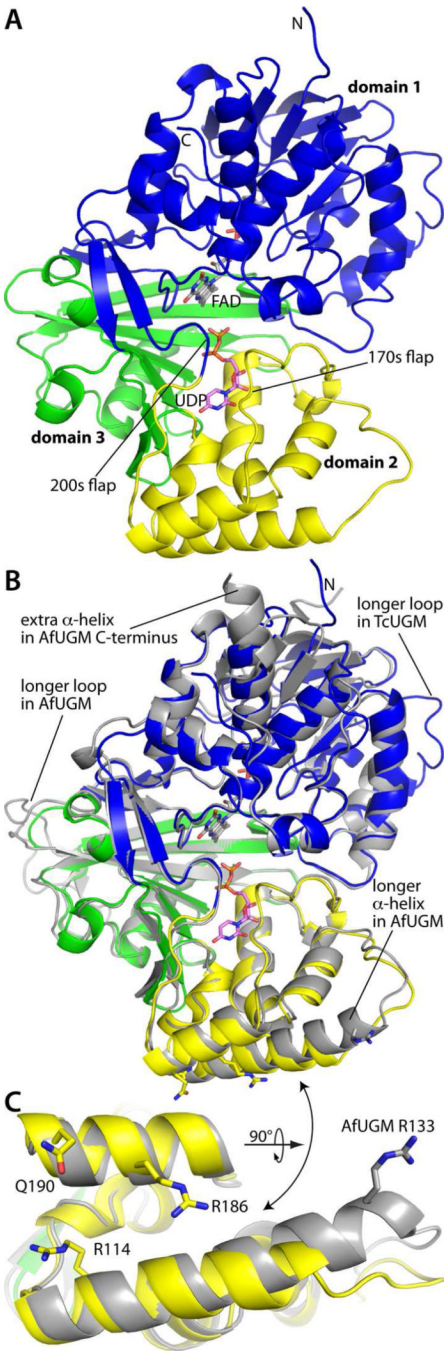

Figure 2.

Structure of TcUGM. (A) Structure of the TcUGM monomer. Domains 1, 2, and 3 are colored blue, yellow, and green, respectively. FAD and UDP are colored gray and pink, respectively. (B) Superposition of TcUGM (blue, yellow, green) and AfUGM (gray). (C) Close-up view of two helices on the periphery of domain 2. The view is rotated from panel B by about 90° around the horizontal axis. TcUGM and AfUGM are colored as in panel B. This figure and others were created with PyMOL (46).

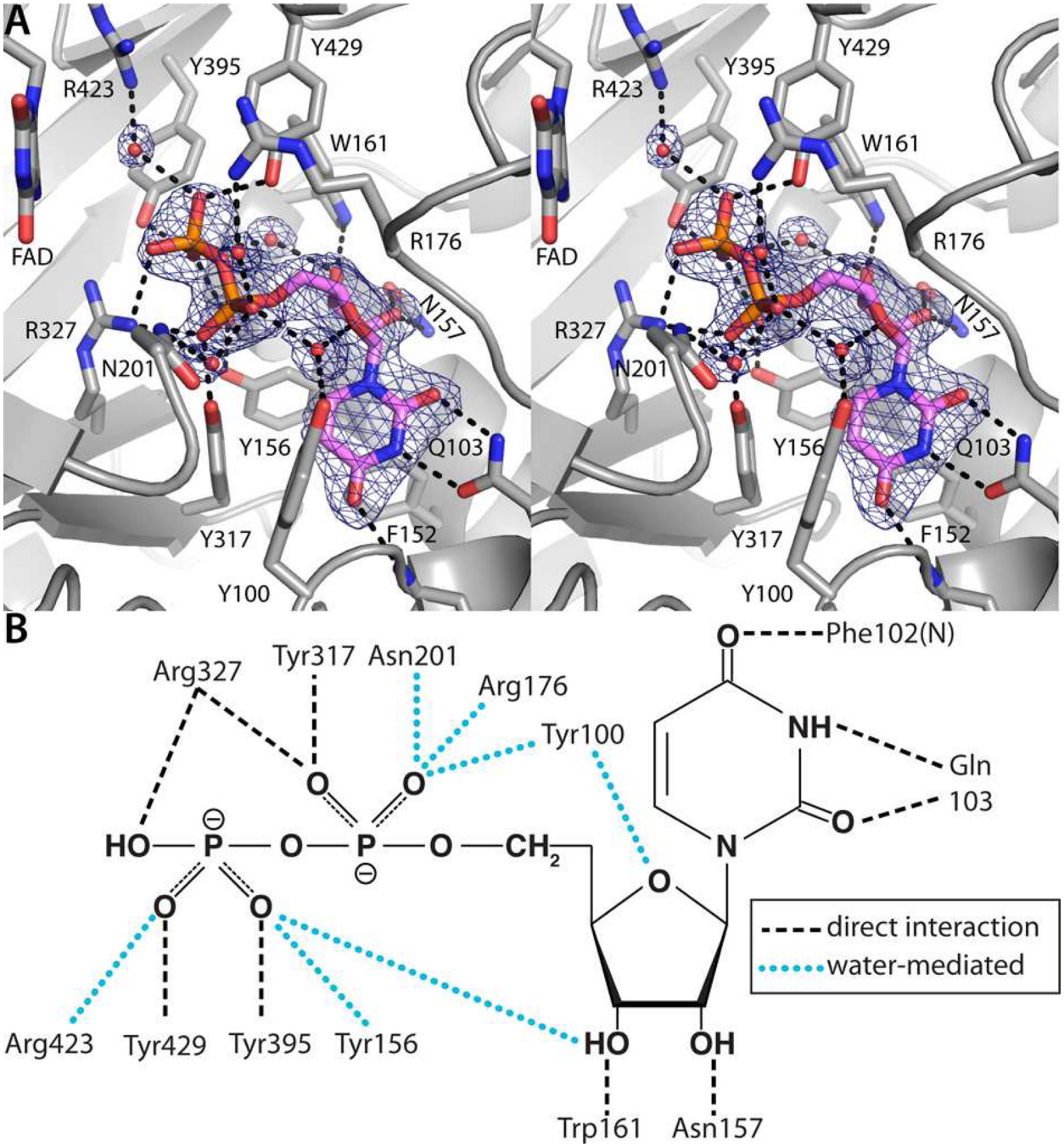

Figure 3.

Electron density and interactions for the UDP bound to reduced TcUGM. (A) Stereographic view of the TcUGM active site. The cage represents a simulated annealing σ_A-weighted $F_o - F_c$ omit map contoured at 3.0 σ. (B) Schematic diagram of protein-UDP interactions in TcUGM. Backbone interactions are indicated by N in parentheses.

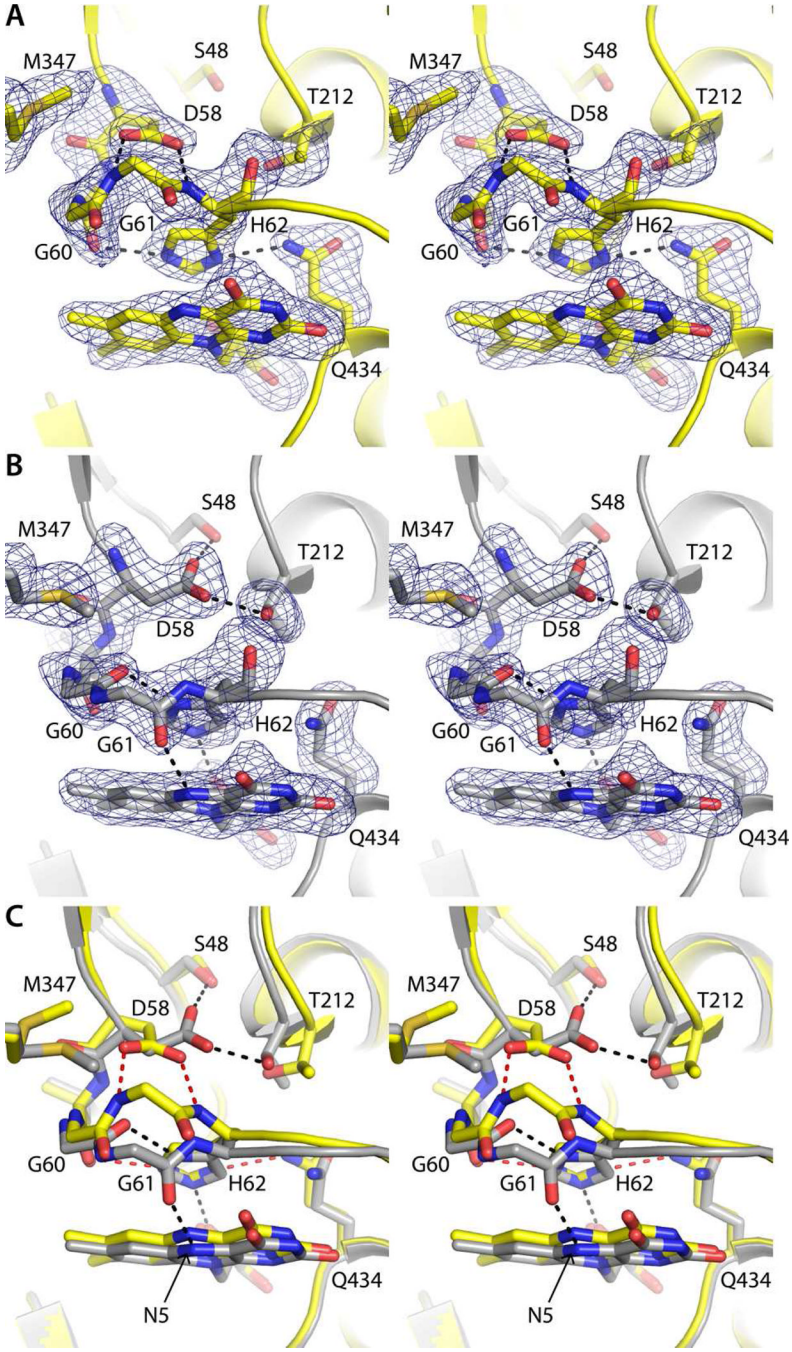

Figure 4.

Structural changes induced by FAD reduction (stereographic views). (A) Electron density for the histidine loop region of oxidized TcUGM. The cage represents a simulated annealing σ_A-weighted $F_o - F_c$ omit map contoured at 3 σ. (B) Electron density for the histidine loop region of reduced TcUGM. The cage represents a simulated annealing σ_A-weighted $F_o - F_c$ omit map contoured at 3 σ. (C) Superposition of oxidized (yellow) and reduced (gray) TcUGM. Red and black dashes represent hydrogen bonds for oxidized and reduced TcUGM, respectively.

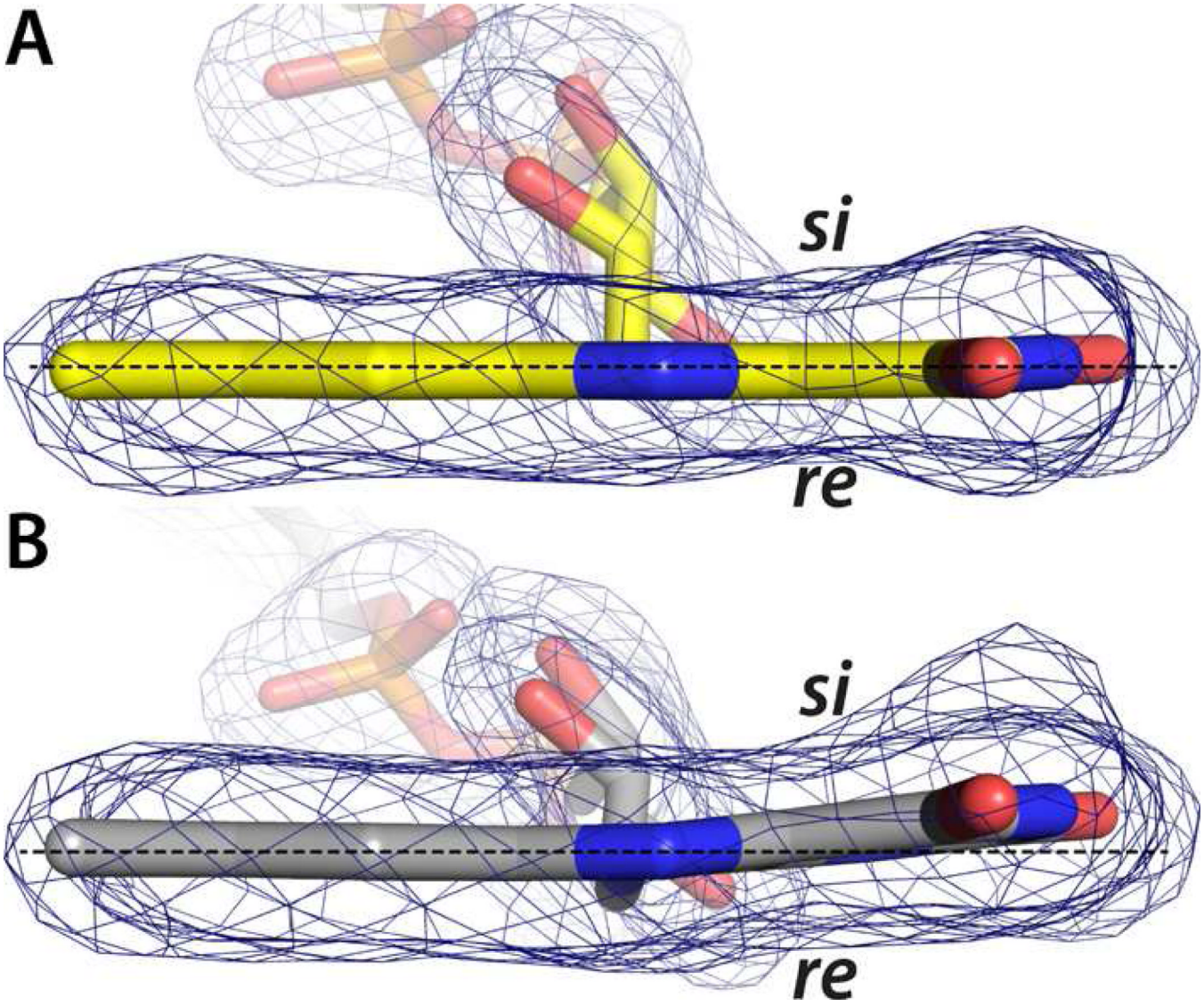

Figure 5.
Electron density for the isoalloxazine rings of (A) oxidized and (B) reduced TcUGM. The cages represent simulated annealing σ_A-weighted $F_o - F_c$ omit maps contoured at 3 σ. The horizontal line assists in seeing the 7° butterfly-like bend angle of the reduced cofactor.

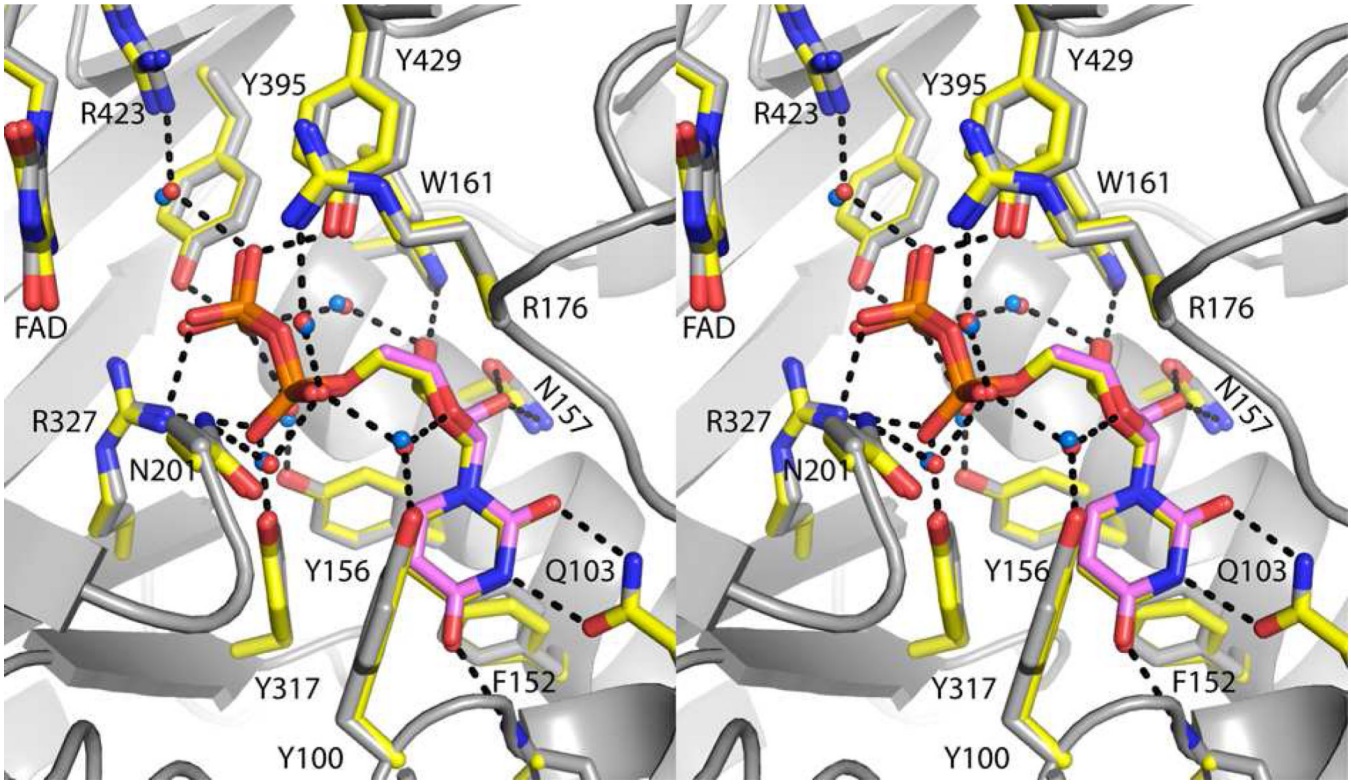

Figure 6.
Superposition of the UDP binding sites of TcUGM and AfUGM (stereographic view). TcUGM is shown with the protein in gray and UDP in pink. AfUGM is colored yellow with blue waters. Note that the two structures are essentially identical, particularly in the region around the uridine.

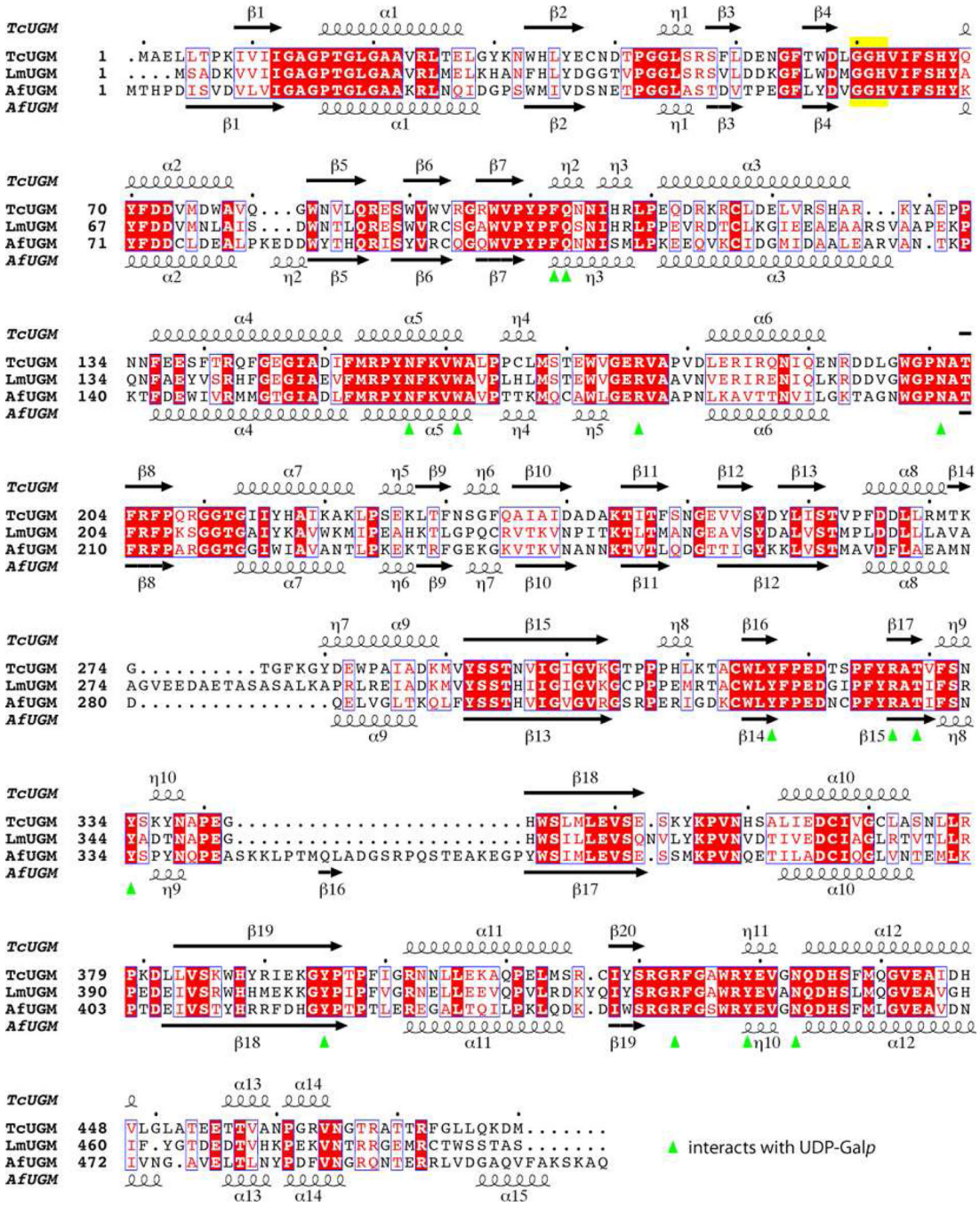

Figure 7.

Amino acid sequence alignment of UGMs from *T. cruzi*, *L. major*, and *A. fumigatus*. The secondary structure elements above and below the alignment are from the TcUGM and AfUGM structures, respectively. The yellow box denotes the histidine loop, which moves in response to changes in the FAD redox state. The green triangles denote residues that contact UDP-Gal*p*; note that they are 100 % identical in the three enzymes.

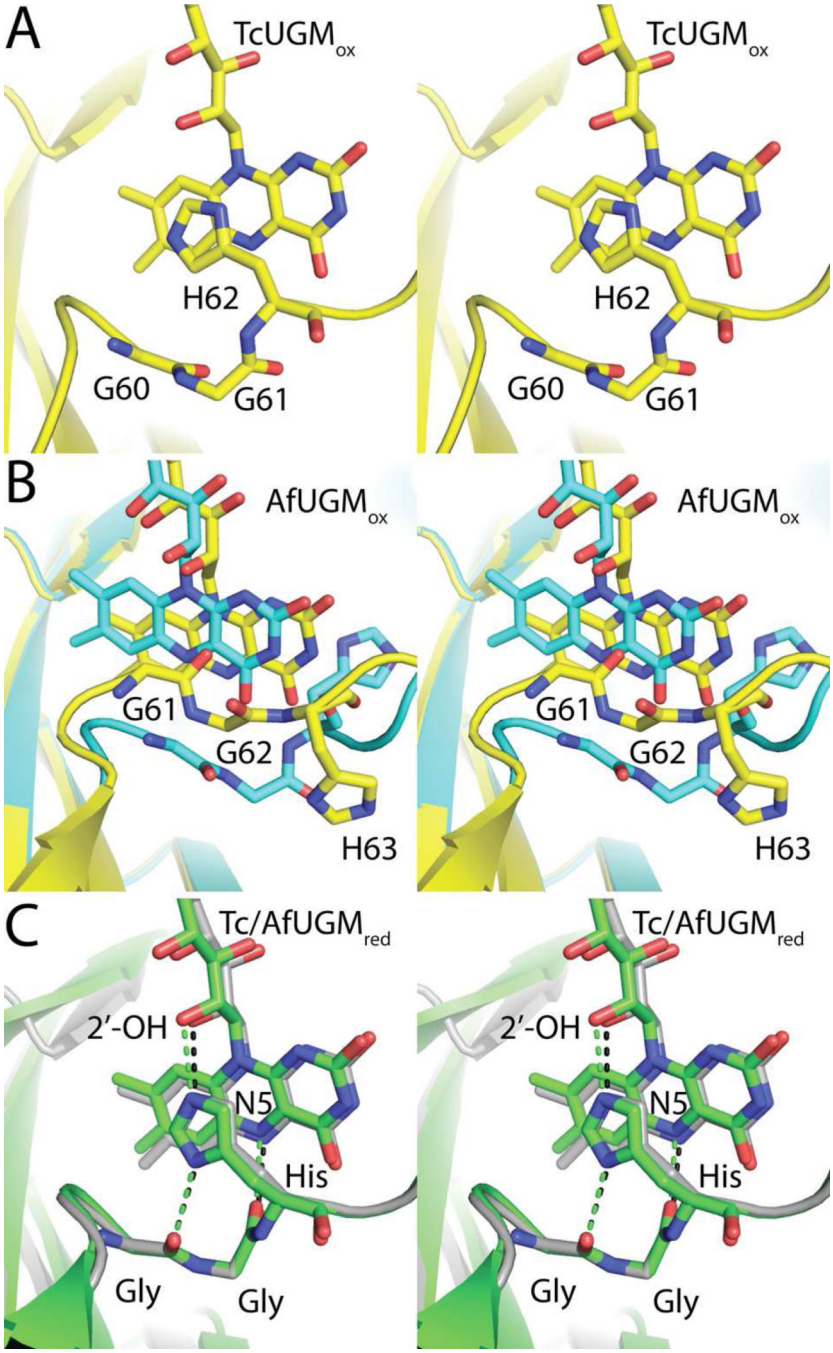

Figure 8.

Summary of conformational changes induced by flavin reduction in TcUGM and AfUGM (stereographic views). (A) Oxidized TcUGM (PDB code 4DSG). (B) Oxidized AfUGM crystallized in space groups $P6_522$ (cyan, PDB code 3UTE) and $P1$ (yellow, PDB code 3UKH). (C) Superposition of reduced TcUGM (gray, 4DSH) and reduced AfUGM (green, 3UTF).

TABLE 1

X-ray Diffraction Data Collection and Refinement[a]

	Oxidized	Reduced
Space group	$P6_522$	$P6_522$
Unit cell parameters (Å)	a = 143.4, c = 354.2	a = 143.8, c = 354.4
Wavelength (Å)	0.9791	0.9795
Resolution (Å)	19.88 - 2.25 (2.33 – 2.25)	47.08 - 2.25 (2.37 – 2.25)
Observations	523354	841035
Unique reflections	101725	102978
$R_{merge}(I)$[b]	0.105 (0.542)	0.089 (0.526)
$R_{meas}(I)$[b]	0.105 (0.647)	0.095 (0.566)
$R_{pim}(I)$[b]	0.045 (0.278)	0.032 (0.204)
Mean I/σ	14.1 (2.2)	17.6 (3.7)
Completeness (%)	99.2 (100.0)	99.9 (99.8)
Multiplicity	5.1 (5.2)	8.2 (7.3)
No. of protein residues	939	938
No. of protein atoms	7495	7482
No. of FAD atoms	106	106
No. of UDP atoms	50	50
No. of water molecules	381	246
R_{cryst}	0.183 (0.246)	0.180 (0.238)
R_{free}[c]	0.212 (0.298)	0.209 (0.283)
rmsd bond lengths (Å)[d]	0.007	0.007
rmsd bond angles (°)[d]	1.12	1.11
Ramachandran plot[e]		
Favored (no. residues)	912	914
Allowed (no. residues)	21	18
Outliers (no. residues)	0	0
Average B-factor (Å^2)		
Protein	30	32
FAD	23	24
UDP	21	25
Water	32	33
Coordinate error (Å)[f]	0.32	0.32
PDB code	4DSG	4DSH

[a] Values for the outer resolution shell of data are given in parenthesis.

[b] Definitions of R_{merge}, R_{meas}, and R_{pim} can be found in Weiss (43).

[c] A common set of test reflections (5 %) was used for refinement of both structures.

[d] Compared to the parameters of Engh and Huber (44).

[e] The Ramachandran plot was generated with RAMPAGE (45).

[f] Maximum likelihood-based coordinate error estimate from PHENIX.

TABLE 2

Steady-state kinetic constants for TcUGM and TcUGM mutant enzymes

	k_{cat} (s^{-1})	K_m (μM)	k_{cat}/K_m (s^{-1} M^{-1})	k_{cat}/K_m (%)
TcUGM[a]	13.4 ± 0.3	140 ± 10	93 ± 6	100 ± 6
G61A	0.198 ± 0.011	50 ± 10	4 ± 1	4 ± 1
G61P	0.83 ± 0.06	90 ± 20	9 ± 2	10 ± 2
H62A	0.041 ± 0.001	24 ± 4	1.8 ± 0.2	2 ± 0.2

[a]Data from Oppenheimer *et al.* (26)